

Mapping of spin wave propagation in a one-dimensional magnonic crystal

César L. Ordóñez-Romero, Zorayda Lazcano-Ortiz, Andrey Drozdovskii, Boris Kalinikos, Melisa Aguilar-Huerta, J. L. Domínguez-Juárez, Guillermo Lopez-Maldonado, Naser Qureshi, Oleg Kolokoltsev, and Guillermo Monsivais

Citation: *Journal of Applied Physics* **120**, 043901 (2016); doi: 10.1063/1.4958903

View online: <http://dx.doi.org/10.1063/1.4958903>

View Table of Contents: <http://scitation.aip.org/content/aip/journal/jap/120/4?ver=pdfcov>

Published by the AIP Publishing

Articles you may be interested in

[Control of elastic wave propagation in one-dimensional piezomagnetic phononic crystals](#)

J. Acoust. Soc. Am. **139**, 3288 (2016); 10.1121/1.4950756

[Spin wave localization in one-dimensional magnonic microcavity comprising yttrium iron garnet](#)

J. Appl. Phys. **116**, 083903 (2014); 10.1063/1.4893936

[Magnetostatic surface wave propagation in a one-dimensional magnonic crystal with broken translational symmetry](#)

Appl. Phys. Lett. **101**, 242408 (2012); 10.1063/1.4771126

[Band structures of exchange spin waves in one-dimensional bi-component magnonic crystals](#)

J. Appl. Phys. **111**, 064326 (2012); 10.1063/1.3698617

[Point defect states of exchange spin waves in all-ferromagnetic two-dimensional magnonic crystals](#)

J. Appl. Phys. **111**, 013908 (2012); 10.1063/1.3673333

A promotional banner for AIP Applied Physics Reviews. The background is a dark blue gradient with a bright light source on the right, creating a lens flare effect. On the left, there is a small image of a book cover for 'AIP Applied Physics Reviews' featuring a diagram of a crystal structure. The main text 'NEW Special Topic Sections' is in large, white, bold font. Below it, 'NOW ONLINE' is in yellow, followed by 'Lithium Niobate Properties and Applications: Reviews of Emerging Trends' in white. The AIP Applied Physics Reviews logo is in the bottom right corner.

NEW Special Topic Sections

NOW ONLINE
Lithium Niobate Properties and Applications:
Reviews of Emerging Trends

AIP Applied Physics
Reviews

Mapping of spin wave propagation in a one-dimensional magnonic crystal

César L. Ordóñez-Romero,^{1,a)} Zorayda Lazcano-Ortiz,¹ Andrey Drozdovskii,^{2,3}
 Boris Kalinikos,^{2,3} Melisa Aguilar-Huerta,¹ J. L. Domínguez-Juárez,⁴
 Guillermo Lopez-Maldonado,⁵ Naser Qureshi,⁶ Oleg Kolokoltsev,⁶
 and Guillermo Monsivais¹

¹Instituto de Física, Universidad Nacional Autónoma de México, CU, México D.F. 04510, Mexico

²St. Petersburg Electrotechnical University, 197376 St. Petersburg, Russia

³International laboratory "MultiferrLab," ITMO University, 197101 St. Petersburg, Russia

⁴Cátedras CONACyT, CFATA, Universidad Nacional Autónoma de México, Juriquilla, Querétaro 76230, Mexico

⁵Universidad Autónoma Metropolitana, Lerma de Villada, 52006 Estado de México, Mexico

⁶CCADET, Universidad Nacional Autónoma de México, CU, México D.F. 04510, Mexico

(Received 10 February 2016; accepted 28 June 2016; published online 22 July 2016)

The formation and evolution of spin wave band gaps in the transmission spectrum of a magnonic crystal have been studied. A time and space resolved magneto inductive probing system has been used to map the spin wave propagation and evolution in a geometrically structured yttrium iron garnet film. Experiments have been carried out using (1) a chemically etched magnonic crystal supporting the propagation of magnetostatic surface spin waves, (2) a short microwave pulsed excitation of the spin waves, and (3) direct spin wave detection using a movable magneto inductive probe connected to a synchronized fast oscilloscope. The results show that the periodic structure not only modifies the spectra of the transmitted spin waves but also influences the distribution of the spin wave energy inside the magnonic crystal as a function of the position and the transmitted frequency. These results comprise an experimental confirmation of Bloch's theorem in a spin wave system and demonstrate good agreement with theoretical observations in analogue phononic and photonic systems. Theoretical prediction of the structured transmission spectra is achieved using a simple model based on microwave transmission lines theory. Here, a spin wave system illustrates in detail the evolution of a much more general physical concept: the band gap. *Published by AIP Publishing.* [<http://dx.doi.org/10.1063/1.4958903>]

I. INTRODUCTION

Periodically structured magnetic materials or magnonic crystals (MCs) have recently demonstrated an outstanding capability to connect fundamental physics with applications in the field of signal engineering at microwave frequencies.^{1–7} In a similar way to their sonic and photonic counterparts, MCs exhibit spin wave dispersion characteristics radically modified with respect to unstructured media.^{8–18} The resulting appearance of frequency band gaps wherein spin wave propagation is prohibited enables a new set of potential applications ranging from microwave filters to a current controlled delay lines and magnon transistors.^{1,5,19} Depending on the desired performance and the final application, magnonic crystals can be implemented from either ferrite or ferromagnetic materials by means of different techniques ranging from chemical etching, metal deposition, ion implantation, or any other method that can create periodical variation of any magnetic parameter.^{20–27} Up until now, however, the best performance characteristics, like small out-of-band insertion losses and deep rejection bands, have been archived by MCs built from a thin yttrium iron garnet (YIG) film with a chemical-etched array of parallel grooves on the surface.¹⁷ Deeper band gaps, low insertion losses, and other unique features of geometrically structured YIG films place these MCs as an excellent choice

to study the linear and nonlinear spin wave dynamics in periodic dispersive media.²⁷

Hitherto, a series of theoretical and experimental studies on magnonic crystals have shown detailed results on the behavior of the frequency-amplitude characteristic as a function of the groove number, depth, and width for all magnetostatic spin wave modes.^{14–18} However, up to now, nothing has been said about the evolution of the spin wave spectrum as a function of the distance inside the magnonic crystal nor about the energy distribution. In this paper, we present a detailed study of the propagation of magnetostatic surface spin waves (MSSWs) through a MC, the formation and the evolution of the frequency band gaps as a function of the propagation distance inside the MC, and the spatial energy distribution as a function of frequency and position. The MC investigated here corresponds to a one-dimensional structure of a YIG film with periodic changes in thickness.

Section II describes the experimental arrangement, including the magnonic crystal fabrication and the magneto-inductive probe measuring set-up. Section III presents the theoretical model used to predict the experimental results. Section IV shows the results and discussion.

II. EXPERIMENT

The magnonic crystal was fabricated using a uniform long and narrow YIG film strip epitaxially grown in the

^{a)}cloro@fisica.unam.mx

(111) crystallographic plane on a gallium gadolinium garnet (GGG) substrate. The YIG strip was 35 mm long, 2 mm wide, and $8.3 \mu\text{m}$ thick with a 5 GHz ferromagnetic resonance half-power line width of about 0.5 Oe. The groove patterning was carried out following a classic photolithographic technique and subsequent hot orthophosphoric acid etching. All the grooves were oriented perpendicular to the spin wave propagation direction. The patterned array was formed with 12 grooves of $70 \mu\text{m}$ width, $1 \mu\text{m}$ depth, and with an interline spacing of $330 \mu\text{m}$, which forms a MC with a lattice constant $a = 400 \mu\text{m}$. The final groove depth profile along the direction of propagation presents a trapezoidal shape due to the typical anisotropic chemical etching of the YIG crystal structure.

The spin wave excitation/detection experimental set up was based on a standard delay line structure and a motorized magneto-inductive probe. Figure 1 illustrates the experimental set up showing the magnonic crystal, the excitation/detection microwave antennas, the magneto-inductive probe, the coordinate system, and the direction of the static external field. For propagation in the MSSW configuration, the static external field H was applied parallel to the surface of the YIG film and perpendicular to the spin wave propagation direction. The field was set up at a nominal value of 770 Oe for all the measurements. To excite and detect the spin waves, a pair of $20 \mu\text{m}$ -diameter gold wire microwave antennas were placed directly on the surface of the YIG film with a separation of 7 mm so that the patterned array of grooves was entirely localized between them. A vector network analyzer connected to these antennas was used to measure the amplitude frequency characteristic of the complete magnonic crystal.

The spatial resolution needed to map the energy of the spin waves in a magnonic crystal was archived by using a motorized magneto inductive probing system. The principle of operation of the magneto-inductive probe is based on Faraday's law of induction and is fine described by Vlannes in Ref. 28. The motorized magnetoinductive system used here was built using a xyz motorized translation stage that moves a coaxial cable with the magnetoinductive probe on the tip. The probe was made using a $20 \mu\text{m}$ diameter gold wire forming a $500 \mu\text{m}$ diameter circular loop. In order to get the strongest signal from the system and map the magnonic crystal response, the probe was set to a fixed position in the

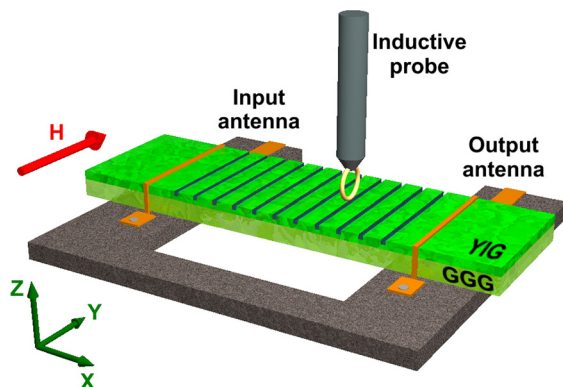


FIG. 1. Diagram of the experimental setup.

yz plane and scanned over the distance between the antennas in the x axis. The probe was placed almost in contact with the film surface in the z direction and in the center of the YIG strip (in the transversal direction, y axis) using an optical microscope. The movement on the x axis was computer-controlled using equal steps of $50 \mu\text{m}$ for all the measurements. It is important to mention that the presence of the probe and its movement along the sample does not affect the shape of the amplitude frequency characteristic nor the results shown in Secs. III–IV.

The propagating MSSWs were pumped by injecting a train of short microwave pulses in the input antenna. The microwave pulses were achieved by modulating a CW microwave oscillator of frequency f with the help of fast p-n diode switch. The duration of the pulses and the repetition rate were set up at 50 ns and 1 kHz to guarantee a spatial profile of the pulses shorter than the magnonic crystal length and no overlapping of pulses, respectively. The detection of the propagating spin wave pulses all over the magnonic crystal was performed by the movable magneto inductive probe and a synchronized fast oscilloscope. With this set up, it was possible to obtain the temporal profile of the transmitted pulse along the propagation path within the range of detectable frequencies of the experimental set up. The range of frequencies was measured using the amplitude frequency characteristic of the complete structure and was set from 3.9 to 4.5 GHz. The swept of frequencies for all measurements was done with increments of 5 MHz.

III. THEORETICAL MODEL

The numerical calculation of the spin wave transmission spectrum was carried out following a similar approach to the theoretical model discussed in Ref. 17. The model treats the scattering of the magnonic crystal considering the patterned structure as a periodic sequence of microwave transmission lines with different propagation constants for a given frequency.²⁹ The spin wave transmission through the MC is then described in terms of a transmission matrix taking interference effects into account in a simplistic way by neglecting the actual trapezoidal shape of the real grooves. Each period of the MC consists in two sections: (1) a plain region of film (PF) and (2) a chemically etched groove with a rectangular cross section (G). The spin wave wavenumber or propagation constant for MSSW is calculated using³⁰

$$k_j = -\frac{1}{2d_j} \ln \left\{ 1 + \frac{4}{\omega_M^2} [\omega_0(\omega_0 + \omega_M) - \omega^2] \right\}, \quad (1)$$

where d_j is the thickness of the film in each section (j could be either PF or G), $\omega_0 = 2\pi|\gamma|H_0$, $\omega_M = 2\pi|\gamma|M_S$, H_0 is the applied magnetic bias field, M_S is the saturation magnetization of YIG, γ is the gyromagnetic ratio, and ω is the spin wave frequency.

To calculate the spatial damping rate in each region, we consider the spin wave loss as due to intrinsic magnetic damping only, which give us

$$k_j' = 2\pi|\gamma|\Delta H/|v_{gj}|, \quad (2)$$

where ΔH is the ferromagnetic resonance half-power line-width and $v_g = \partial\omega/\partial k$ is the spin wave group velocity for MSSW given by

$$v_{gj} = \frac{\omega_M^2 d_j}{4\omega} e^{-2k_j d_j}. \quad (3)$$

Using these expressions, the matrices that describe the spin wave propagation either in the unstructured regions or inside the grooves are given by

$$T_j = \begin{pmatrix} e^{-(ik_j - k'_j)L_j} & 0 \\ 0 & e^{(ik_j - k'_j)L_j} \end{pmatrix}, \quad (4)$$

where L_j is the length of the corresponding region. Now, regarding the transmission effects at the edges of the grooves, it is expected that the incident wave will be partially reflected back. This condition of reflection at edges has to be taken into account and can be represented by means of two additional matrices of the form

$$T_\nu = \begin{pmatrix} (1 - \nu\Gamma)^{-1} & \nu\Gamma(1 - \nu\Gamma)^{-1} \\ \nu\Gamma(1 - \nu\Gamma)^{-1} & (1 - \nu\Gamma)^{-1} \end{pmatrix}, \quad (5)$$

where Γ is the reflection coefficient and ν is the direction index. $\nu = +1$ has to be used for the front edge (i.e., when the spin wave is coming from the unstructured section of the film towards the groove), and $\nu = -1$ for the rear edge (where the wave incident onto the same interface is coming from the opposite direction).

Since the grating has been treated as a periodic sequence of microwave transmission lines, it is reasonable to define Γ in terms of a difference of the “characteristic impedance” of the YIG film. Assuming the influence of the change of the YIG film thickness as a variation of the film’s effective inductance, the “characteristic impedance” of the magnonic waveguide is then linearly proportional to k , and therefore, Γ can be written in terms of the thicknesses: $\Gamma = (d_{PF} - d_G)/(d_{PF} + d_G)$. If δ is the depth of the grooves, then $\Gamma = \delta/(2d_{PF} - \delta)$.

Finally, using the transmission matrix properties, the propagation through a complete period can be analyzed by multiplying the matrices, $T = [T_{PF} \cdot T_+ \cdot T_G \cdot T_-]$, and, for the complete MC with N periods, the total matrix will be given by T to the N -th power $T^{MC} = [T]^N$. Wherefrom the power transmission coefficient of the magnonic crystal can be determined as $P_{tr} = 1/|T_{11}^{MC}|^2 = 1/|T_{22}^{MC}|^2$.

The MSSW modes present the field displacement non-reciprocity effect that shifts the maximum of the magnetostatic potential from one surface to the other when reversing the direction of propagation. However, this effect is a gradually developing phenomenon that depends on the spin wave wavenumber.³⁰ For small wavenumbers $kd < 1$, where d is the film thickness, the effect is very weak and can be neglected in the current theoretical model to predict the formation of spin wave band gaps as will be shown in Sec. IV.

IV. RESULTS AND DISCUSSION

Figure 2 shows representative data on the transmission spin wave spectrum along the magnonic crystal. The 3D

surface represents the normalized intensity of spin waves as a function of transmitted frequency and propagation distance inside the magnonic crystal. The normalized intensity of the spin waves for each position and frequency was calculated by integrating the square of the corresponding temporal profile of the measured propagating spin wave pulse. The integration interval is 1 μ s for all the cases. Given the symmetry of the system, the transmission properties do not depend on variable y . Therefore, a trace in one spatial dimension was sufficient to characterize the propagation. The probe position axis represents the range of scanned positions by the magnetoinductive probe. The step size for all the measurements was 50 μ m. The position of the input and output antennas was one millimeter away from the initial and the final scanned points, respectively. For clarity, the inset in Fig. 2 shows representative oscilloscope traces corresponding to the envelope of the spin wave pulses measured for two different excitation frequencies and three different positions along the propagation path.

Figure 2 reveals the effect of the periodic structure in the spin wave transmission spectrum. As expected, close to the excitation antenna, a surface cut plot at $x = 0$ shows a distinctive MSSW transmission spectrum with maximum amplitude at low frequencies and the characteristic smooth intensity drop as frequency increases. In contrast, at the edge of the magnonic crystal (5 mm), the amplitude frequency characteristic shows the presence of a set of band gaps where the spin waves with those particular frequencies have experienced stronger attenuation assets. The appearance of these characteristic band gaps is the signature of the magnonic crystal influence in the spin wave propagation. It is clear from Fig. 2 that the formation of these rejection bands is a progressive effect rather than an instantaneous one, and the spin wave transmission spectrum shows deeper rejection bands at positions where the propagating spin waves have been transmitted through a larger number of grooves.

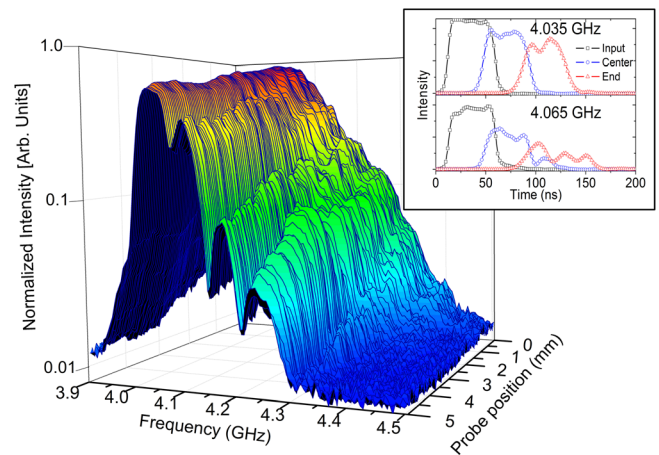


FIG. 2. Normalized intensity distribution of spin waves as a function of transmitted frequency and the propagation distance in a magnonic crystal. The 3D surface plot was calculated by integrating the square of the corresponding temporal profile of the measured propagating spin wave pulse for each position and frequency. The intensity is displayed in logarithmic scale. Inset: Temporal profiles of the spin wave pulse envelope measured at the input, at the center, and at the end of the periodic structure for two different frequencies corresponding to a transmission band (4.035 GHz) and a band gap (4.065 GHz).

Displaying the data in a different way, Fig. 3(a) shows a contour plot of Fig. 2. The normalized intensity of spin waves as a function of transmitted frequency and propagation distance in the magnonic crystal is now displayed using a color palette in a 2D plot with the same axes of Fig. 2. The photograph of the magnonic crystal located on the top of Fig. 3(a) shows the real position of the MC relative to the horizontal axis. Figure 3(b) shows both the experimental (red line) and theoretical (black line) amplitude frequency characteristic for the complete periodic structure. The red line was measured in CW regime using a vector network analyzer connected to the input and output antennas; meanwhile, the black line represents the theoretical prediction of the transmission spectrum based on the theory described above. Figure 3(c) shows the experimental spin wave dispersion relation in the magnonic crystal. This frequency vs. wavenumber graph was obtained by measuring the phase change as a function of frequency between the input and output antennas. The position and scale of the frequency axes of Figs. 3(b) and 3(c) were chosen to match with the vertical axis of Fig. 3(a) and allow an easier comparison. Figures 3(a) and 3(b) are plotted using logarithmic scale for intensity. Horizontal dashed arrows are introduced in the figure to link the band gaps with observable changes in the spin wave dispersion curve. The small dotted square in Fig. 3(c) indicates the portion of the dispersion relation plotted in the figure inset.

In contrast to Fig. 2, Fig. 3(a) shows clearly not only the formation of the spin wave band gaps but also the influence of

the periodic structure in the distribution of the spin wave energy as a function of the transmitted frequency and position inside the magnonic crystal. Regarding the first outcome, it is clear from the figure that the formation of the band gaps is inclusively confirmed by the spin wave dispersion relation. Even though it is hardly observable from the full scale Fig. 3(c), the inset shows that the influence of the periodic structure in the spin wave mode is present for all band gaps in the form of severe changes of the spin wave group velocity $\partial\omega/\partial k$. Thus, it is possible to claim that the theoretical prediction (black line), the measured amplitude frequency characteristic of the complete magnonic structure (red line), the spin wave relation dispersion, and the constructed spin wave intensity map (contour plot) present good agreement in central frequency and bandwidth of the observable band gaps. It is important to mention that for frequencies above 4.3 GHz, the signal intensity at the magnetoinductive probe is so small that the measuring system does not have the sensitivity to resolve the propagating signal. This is the reason why the contour plot shows only noise above this frequency. Moreover, the first expected bandgap at π/a (78.5 rad/cm) is not observable based on the fact that the excitation efficiency of the antenna for spin waves with wavenumbers below 100 rad/cm is very low, and thus, we cannot excite the first transmission band.

On the other hand, Fig. 3(a) shows that the periodic structure modifies the way the energy is distributed along the propagation path. It is clear from the figure that, for frequencies above 4.2 GHz, the intensity plot exposes the localization of the grooves showing minima in the contour plot. However, this

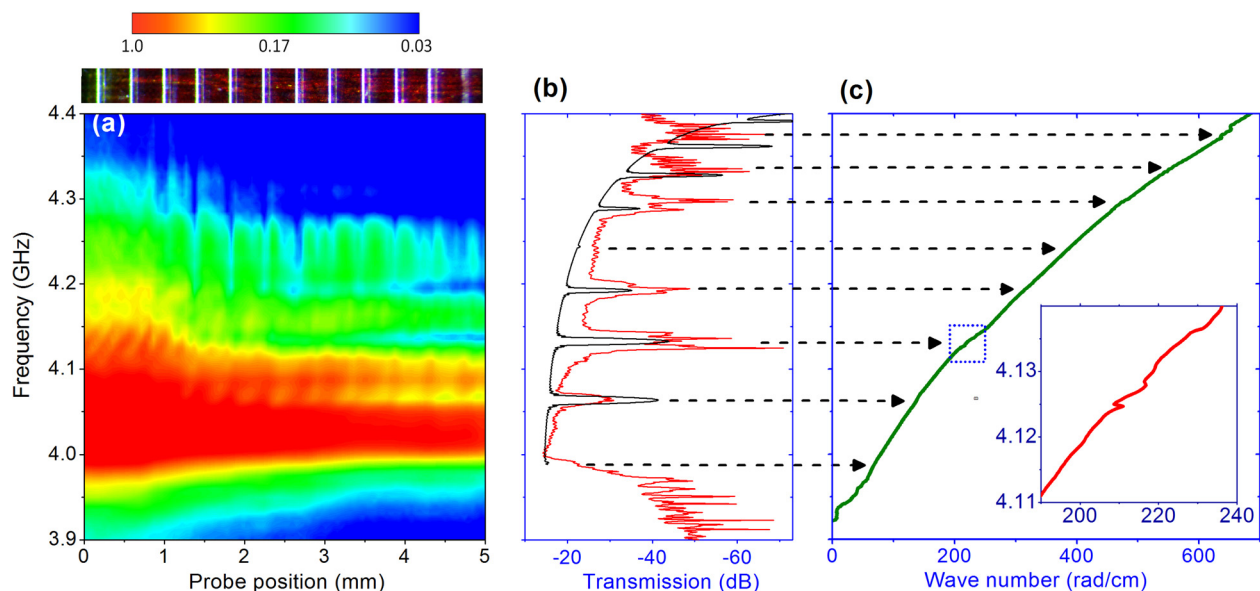


FIG. 3. Experimental signature of the formation of spin wave band gaps in a magnonic crystal. (a) Contour plot of the spin wave transmission spectra as a function of the propagation distance in a magnonic crystal. The photograph of the magnonic crystal located on the top shows the real position of the MC relative to the horizontal axis. (b) Experimental (red line) and theoretical (black line) spin wave transmission spectrum of the complete magnonic crystal. The red line curve was measured using a vector network analyzer connected to the input and output antennas, meanwhile the black line represents the theoretical prediction of the transmission spectrum based on the theory described in Section III. Both figures are plotted using a logarithmic scale. The theoretical prediction was carried out using the following parameters: $d_{PF} = 8.3 \mu\text{m}$, $\delta = 1 \mu\text{m}$, $L_{PF} = 330 \mu\text{m}$, $L_G = 70 \mu\text{m}$, $\Delta H = 0.5 \text{Oe}$ (the accuracy of the measurement of ΔH is consistent over the frequency range used in the simulation), $\gamma = 2.8 \text{MHz/G}$, $M_s = 1750 \text{G}$ and $H_0 = 770 \text{Oe}$. (c) Experimental spin wave relation dispersion of the magnonic crystal obtained by measuring the phase change between the antennas. The horizontal arrows are introduced to link the position of the expected band gaps at $k = n\pi/a$ (with $n = 1, 2, \dots$) in Figure 3(b) with the changes in slope in the spin wave relation dispersion. The dotted square indicates the portion of the spin wave relation dispersion plotted in the figure inset. The frequency axes in Figures 3(b) and 3(c) contain the same scale and position on the one in Figure 3(a) to allow an easier comparison.

outcome has to be taken with reserve because it is not true for all the frequencies and it is necessary to display the data in a different way to observe this interesting result.

Following with this discussion, Fig. 4 shows data of the spatial evolution of the normalized intensity of spin waves along the magnonic crystal for a series of particular frequencies. Red lines correspond to frequencies of maximum transmission in the first four observed transmission bands meanwhile blue lines correspond to frequencies of minimum transmission in the first four observable band gaps. All the graphs are plotted using logarithmic intensity scale and the same linear horizontal axis. The position of the magnonic crystal grooves is indicated with the vertical dotted lines.

One of the first observables from Fig. 4 is the evident difference in the attenuation effects suffered by the spin waves with frequencies coinciding with the transmission bands in comparison to those from the rejection bands. The slope of the red lines represents the spin wave attenuation behavior in linear regime for propagating spin waves in the transmission bands. In contrast, it is clear from the blue lines that the damping mechanism in the band gaps presents an additional contribution from the periodic media that changes the spatial profiles of the intensity drastically. This additional damping mechanism depends exclusively on the magnonic structure and it can be manipulated by tailoring the parameters of the geometric structure.¹⁷

Another interesting observable is the spatial modulation of the intensity. It is clear from Fig. 4(a) that the spatial profiles from the first observable bands (transmission and

rejection) show an oscillatory spatial modulation of the intensity with a period coinciding with the groove spacing, showing maxima in the grooves and minima in the unstructured part of the film. Simultaneously, Fig. 4(b) shows a similar situation regarding the location of the maxima but this time presenting a shorter period of the oscillatory behavior of the intensity. This outcome is expected since these frequencies correspond to transmission or rejection bands of higher order. Keeping in mind this trend, one would expect that the subsequent bands, again transmission and rejection, will show even a higher order in the oscillatory behavior. However, this situation is not clearly shown by Figs. 4(c) and 4(d) due to a limited spatial resolution of the measuring technique. What is clear is that for these bands the energy distribution changes and now shows minima at the groove positions. These two interesting outcomes, the oscillatory characteristic of the energy along the propagation path and the peculiar localization of the maxima in the magnonic structure, represent the first direct experimental observation of the Bloch theorem for a spin wave system. According to Bloch's theorem, the functions that describe the behavior of the propagating waves in a periodic structure will always have the form³¹

$$\Psi^{(k)}(x) = u_p^{(k)}(x) e^{ikx}, \quad (6)$$

with a magnitude given by

$$|\Psi^{(k)}(x)| = |u_p^{(k)}(x)|, \quad (7)$$

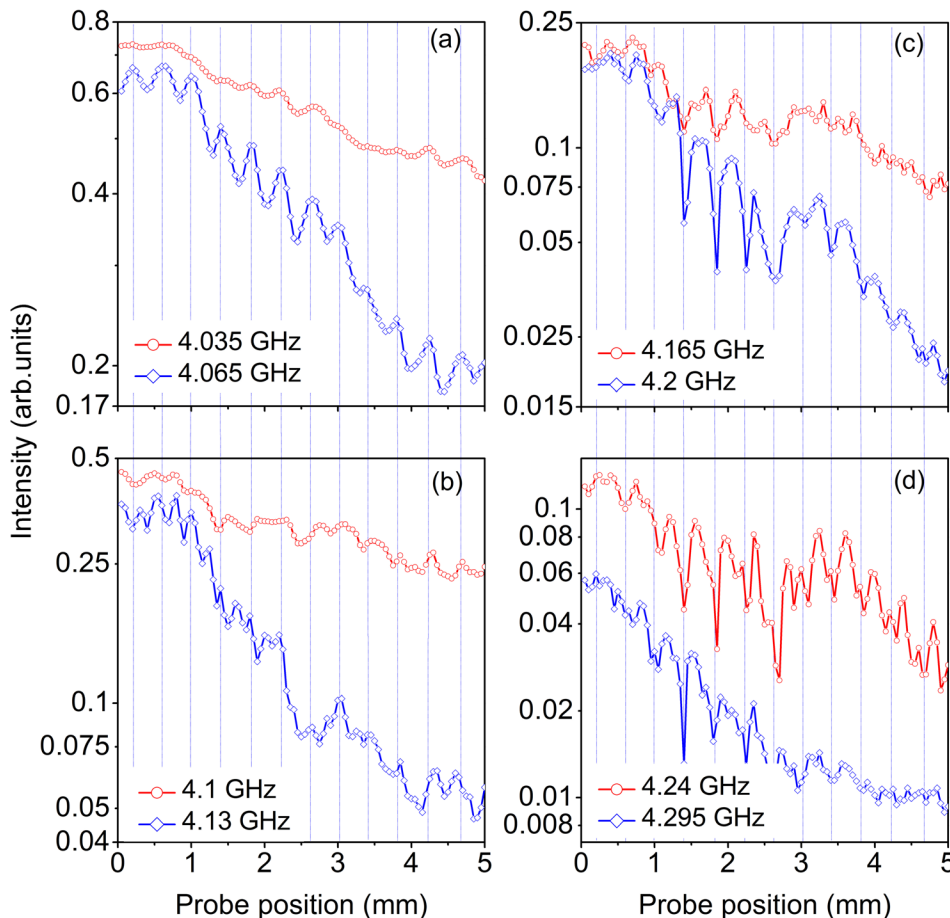


FIG. 4. Spatial evolution of the normalized intensity of spin waves along the magnonic crystal. (a) Spatial decay of spin wave from the first (a), second (b), third (c), and fourth (d) transmission (red lines) and rejection (blue lines) bands. All the vertical axes are logarithmic scale. Vertical dotted blue lines indicate the position of the chemically etched grooves.

where p is the period of the structure and $u_p^{(k)}(x)$ is a periodic function with a period p . This means that the function that describes the intensity of the propagating wave $\Psi^{(k)}(x)$ will also present the same periodic dependence, showing an oscillatory characteristic along the propagation path.^{32–35} Now, regarding the positions of the maxima and minima of the energy, studies in quantum, phononic, and photonic periodic systems have shown that the positions of maxima and minima depend in a very complicated manner on the geometry and composition of the system. Thus, in our case, we also expect a complex energy distribution that behaves in a different way for each transmission or rejection band. This direct experimental confirmation of Bloch's theorem reported here shows how spin wave technology provides an easy way to elucidate the physics behind similar problems in analogue systems such as photonic and phononic crystals.^{36–38}

V. CONCLUSION

In this work, we experimentally map the formation and evolution of the spin wave transmission spectrum in a 1D magnonic crystal in the MSSW configuration. The resultant amplitude frequency characteristic shows the appearance of frequency band gaps wherein spin wave propagation exhibits a signal rejection larger than 20 dB. As shown in the energy distribution map, this overdamping mechanism induced by the periodic structure is a progressive effect rather than instantaneous. This implies that the spin wave transmission spectrum will show deeper band gaps when transmitted through a larger number of grooves. This spatial evolution of the band gap is likely a general characteristic of photonic and phononic crystal structures and is illustrated in a particularly explicit fashion in this magnonic system.

Another interesting result is the experimental observation of the spatial intensity distribution for all the frequencies. We experimentally demonstrate an interesting oscillatory behavior of the normalized intensity for all observable bands (transmission and rejection), showing that the position of maxima and minima as well as the period of the oscillatory characteristic is linked with the order of the band gaps and reflects once more the influence of the periodic structure in the propagation of the spin waves. More generally, this result offers a direct experimental confirmation of the validity of Bloch's theorem in a spin wave system.

ACKNOWLEDGMENTS

This work has been supported by UNAM-DGAPA Grant No. 1N103915 and postdoctoral fellowship, by Catedras Conacyt Grant No. 1069 and by the Government of the Russian Federation (Grant No. 074-U01 and project "Goszadanie").

¹K. W. Reed, J. M. Owens, and R. L. Carter, *Circuits Syst. Signal Process* **4**, 157 (1985).

- ²A. B. Ustinov, N. Yu. Grigor'eva, and B. A. Kalinikos, *JETP Lett.* **88**, 31 (2008).
- ³A. V. Drozdovskii and B. A. Kalinikos, *JETP Lett.* **95**, 357 (2012).
- ⁴A. B. Ustinov, B. A. Kalinikos, V. E. Demidov, and S. O. Demokritov, *Phys. Rev. B* **81**, 180406(R) (2010).
- ⁵A. B. Ustinov, A. V. Drozdovskii, and B. A. Kalinikos, *Appl. Phys. Lett.* **96**, 142513 (2010).
- ⁶A. V. Chumak, V. S. Tiberkevich, A. D. Karenowska, A. A. Serga, J. F. Gregg, A. N. Slavin, and B. Hillebrands, *Nat. Commun.* **1**, 141 (2010).
- ⁷A. D. Karenowska, A. V. Chumak, A. A. Serga, J. F. Gregg, and B. Hillebrands, *Appl. Phys. Lett.* **96**, 082505 (2010).
- ⁸Yu. V. Gulyaev and S. A. Nikitov, *Dokl. Phys.* **46**, 687 (2001).
- ⁹C. G. Sykes, J. D. Adam, and J. H. Collins, *Appl. Phys. Lett.* **29**, 388 (1976).
- ¹⁰J. P. Parekh and H. S. Tuan, *Appl. Phys. Lett.* **30**, 667 (1977).
- ¹¹J. P. Parekh and H. S. Tuan, *IEEE Trans. Microwave Theory Tech.* **26**, 1039 (1978).
- ¹²J. Gouzerh, A. A. Stashkevich, N. G. Kovshikov, V. V. Matyushev, and J. M. Desvignes, *J. Magn. Magn. Mater.* **101**, 189 (1991).
- ¹³P. A. Kolodin and B. Hillebrands, *J. Magn. Magn. Mater.* **161**, 199 (1996).
- ¹⁴A. V. Chumak, T. Neumann, A. A. Serga, B. Hillebrands, and M. P. Kostylev, *J. Phys. D: Appl. Phys.* **42**, 205005 (2009).
- ¹⁵A. V. Chumak, A. A. Serga, B. Hillebrands, and M. P. Kostylev, *Appl. Phys. Lett.* **93**, 022508 (2008).
- ¹⁶A. V. Chumak, A. A. Serga, S. Wolff, B. Hillebrands, and M. P. Kostylev, *Appl. Phys. Lett.* **94**, 172511 (2009).
- ¹⁷A. V. Chumak, A. A. Serga, S. Wolff, B. Hillebrands, and M. P. Kostylev, *J. Appl. Phys.* **105**, 083906 (2009).
- ¹⁸F. Ciubotaru, A. V. Chumak, B. Obry, A. A. Serga, and B. Hillebrands, *Phys. Rev. B* **88**, 134406 (2013).
- ¹⁹A. V. Chumak, A. A. Serga, and B. Hillebrands, *Nat. Commun.* **5**, 4700 (2014).
- ²⁰Y. Filimonov, E. Pavlov, S. Vystostkii, and S. Nikitov, *Appl. Phys. Lett.* **101**, 242408 (2012).
- ²¹Y. Zhu, K. H. Chi, and C. S. Tsai, *Appl. Phys. Lett.* **105**, 022411 (2014).
- ²²P. J. Metaxas, M. Sushruth, R. A. Begley, J. Ding, R. C. Woodward, I. S. Maksymov, M. Albert, W. Wang, H. Fangohr, A. O. Adeyeye, and M. Kostylev, *Appl. Phys. Lett.* **106**, 232406 (2015).
- ²³M. Krawczyk and D. Grundler, *J. Phys.: Condens. Matter* **26**, 123202 (2014).
- ²⁴B. Lenk, H. Ulrichs, F. Garbs, and M. Münzenberg, *Phys. Rep.* **507**, 107 (2011).
- ²⁵V. V. Kruglyak, S. O. Demokritov, and D. Grundler, *J. Phys. D: Appl. Phys.* **43**, 264001 (2010).
- ²⁶M. Vogel, A. V. Chumak, E. H. Waller, T. Langner, V. I. Vasyuchka, B. Hillebrands, and G. von Freymann, *Nat. Phys.* **11**, 487 (2015).
- ²⁷A. A. Serga, A. V. Chumak, and B. Hillebrands, *J. Phys. D: Appl. Phys.* **43**, 264002 (2010).
- ²⁸N. P. Vlannes, *J. Appl. Phys.* **61**(1), 416 (1987).
- ²⁹A. Maeda and M. Susaki, *IEEE Trans Magn.* **42**, 3096 (2006).
- ³⁰D. D. Stancil and A. Prabhakar, *Spin Waves: Theory and Applications* (Springer, New York, 2009).
- ³¹C. Kittel, *Introduction to Solid State Physics* (John Wiley and Sons, New York, 1996).
- ³²M. L. Sokolovskyy and M. Krawczyk, *J. Nanopart. Res.* **13**, 6085 (2011).
- ³³K.-S. Lee, D.-S. Han, and S.-K. Kim, *Phys. Rev. Lett.* **102**, 127202 (2009).
- ³⁴M. Kostylev, P. Schrader, R. L. Stamps, G. Gubbiotti, G. Carlotti, A. O. Adeyeye, S. Goolaup, and N. Singh, *Appl. Phys. Lett.* **92**, 132504 (2008).
- ³⁵M. Mruczkiewicz, E. S. Pavlov, S. L. Vysotsky, M. Krawczyk, Yu. A. Filimonov, and S. A. Nikitov, *Phys. Rev. B* **90**, 174416 (2014).
- ³⁶K. Sakoda and H. Shiroma, *Phys. Rev. B* **56**, 4830 (1997).
- ³⁷E. Almpanis, N. Papanikolaou, and N. Stefanou, *Opt. Express* **22**, 31595 (2014).
- ³⁸E. Descrovi, C. Ricciardi, F. Giorgis, G. Lérondel, S. Blaize, C. X. Pang, R. Bachelot, P. Royer, S. Lettieri, F. Gesuele, P. Maddalena, and M. Liscidini, *Opt. Express* **15**, 4159 (2007).